Inorganic Chemistry

Article

pubs.acs.org/IC

Synthesis and Electrochemical Reactivity of Molybdenum Dicarbonyl Supported by a Redox-Active α-Diimine Ligand

Isaac R. Corn,[†] Pablo D. Astudillo-Sánchez,[†] Michael J. Zdilla,[†,‡] Phillip E. Fanwick,[†] Michael J. Shaw,[§] Jeffrey T. Miller,[⊥] Dennis H. Evans,*[,†] and Mahdi M. Abu-Omar*[,†]

[†]Brown Laboratory, Department of Chemistry, Purdue University, 560 Oval Drive, West Lafayette, Indiana 47907, United States

[§]Department of Chemistry, Southern Illinois University at Edwardsville, Edwardsville, Illinois 62026, United States

[⊥]Chemical Sciences and Engineering Division, Argonne National Laboratory, 9700 South Cass Avenue, Argonne, Illinois 60439, United States

Supporting Information

ABSTRACT: Low-valent molybdenum dicarbonyl complexes with a diazabutadiene [$^{mes}DAB^{R}$; [ArN═C(R)C(R)═NAr]; Ar = 2,4,6-trimethylphenyl (mes), R = H or CH_3] ligand have been synthesized and fully characterized. The title complexes exhibit elongated DAB C−N and shortened C−C bond lengths over the free ligand and other zerovalent molybdenum complexes of DAB. Compared to known examples theoretically described as iminato π-radicals ($L^{\bullet-}$), the oxidation state assignment fits a molybdenum(II) description. However, Mo K-edge X-ray absorption spectroscopy indicates that the complexes are best described as molybdenum(0). This example demonstrates that caution should be exercised in assigning the oxidation state based on structural parameters alone. Cyclic voltammetry studies reveal an electrochemical−chemical process that has been identified by in situ Fourier transform infrared spectroelectrochemistry as cis-to-trans isomerization.

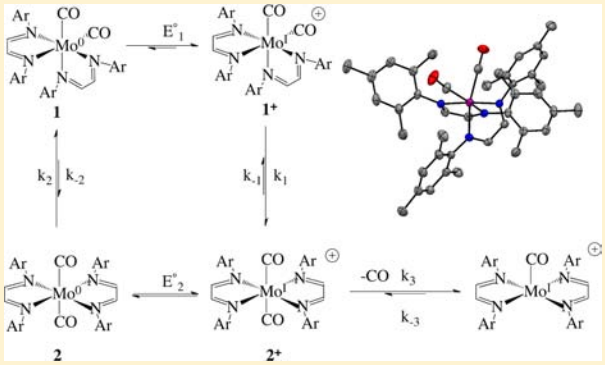

INTRODUCTION

Noninnocent redox-active ligands have gained renewed attention in the literature because their coordination complexes are rich in bonding and electronic structure.[1−4] New reactivities of their complexes have been exploited based on the ligand's ability to act as a reservoir for electrons,[5−8] allowing, for example, reductive elimination and small-molecule activation on d^0 metal centers.[9−11] 1,4-Diaza-1,3-butadiene (DAB) ligands have been widely studied in olefin polymerization,[12−14] in atom-transfer-radical polymerization,[15−17] and for their electronic properties.[18−21] These ligands can store up to two electrons and are thought to be present as α-diimine (0), iminate π radical (1−), or α-diamide (2−).[22−25] The form of the ligand is characterized by the C−N and C−C bond lengths (see Scheme 1).[26,27]

While there are many examples of α-diimine-supported molybdenum(0) carbonyls, the current literature focuses mainly on tetracarbonyl, tricarbonylsolvato, and bipyridyl complexes.[28,29] In this paper, we describe the synthesis and characterization of molybdenum dicarbonylbis(1,4-diaza-1,3-butadiene) complexes. Much of the literature places an emphasis on the ability to establish a correlation between the DAB bond lengths and the oxidation state of the metal, and indeed for most examples, such a correlation holds true. Structural data for the reported complexes herein are in agreement with a formal molybdenum(II) metal center and monoanionic iminate π radical (1−) DAB ligands. However, Mo K-edge X-ray absorption near-edge structure (XANES) indicates that the oxidation state is molybdenum(0). Spectroscopic and computational data suggest significant covalency with the electron density shared in orbitals spanning both ligands and the metal center. Electrochemical investigations reveal a one-electron oxidation followed by a chemical process. The latter has been identified as an isomerization based on difference Fourier transform infrared (FTIR) spectroelectrochemistry.

Scheme 1. Structural Features of the DAB Ligand in Its Three Recognized States as α-Diimine (0), Iminate π Radical (1−), or α-Diamide (2−)

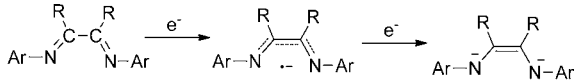

C-C (Å)	1.47	1.38	1.36
C-N (Å)	1.29	1.34	1.40

Received: February 13, 2013
Published: April 11, 2013

   dx.doi.org/10.1021/ic400348j | Inorg. Chem. 2013, 52, 5457−5463

Table 1. X-ray Crystallographic Parameters

	1	3	4	5
formula	$C_{42}H_{48}MoN_4O_2$	$C_{46}H_{56}Mo_1N_4O_2$	$C_{26}H_{28}MoN_2O_4$	$C_{25}H_{27}MoN_3O_3$
fw	736.82	792.92	528.46	513.45
space group	$P\bar{1}$ (No. 2)	$P2/n$ (No. 13)	$Pbca$ (No. 61)	$P2_1/c$ (No. 14)
a (Å)	11.0982(12)	15.4335(11)	8.4968(5)	15.2745(10)
b (Å)	11.1809(14)	8.9648(7)	20.4430(12)	7.6639(4)
c (Å)	17.421(4)	16.7602(13)	28.4906(13)	21.9287(14)
α (deg)	101.38(2)	90	90	90
β (deg)	95.65(3)	92.030(6)	90	110.075(2)
γ (deg)	117.05(2)	90	90	90
V (Å^3)	1842.6(5)	2317.5(3)	4948.8(5)	2411.1(3)
T (K)	150	150	150	150
λ (Å)	0.71073	1.54184	1.54184	0.71073
ρ (g cm^{-3})	1.328	1.136	1.418	1.414
μ (mm^{-1})	0.385	2.595	4.675	0.559
transm coeff	0.716–0.981	0.925–0.925	0.509–0.869	0.819–0.956
R (F_o)^a	0.071	0.069	0.057	0.071
R_w (F_o^2)^b	0.159	0.186	0.158	0.181

$^aR = \sum||F_o| - |F_c||/\sum|F_o|$ for $F_o^2 > 2\sigma(F_o^2)$. $^bR_w = [\sum w(|F_o^2| - |F_c^2|)^2/\sum w|F_o^2|^2]^{1/2}$.

EXPERIMENTAL SECTION

All solvents were dried by distillation over sodium/benzophenone or by a solvent purification system (Anhydrous Engineering Inc.), degassed, and stored over molecular sieves prior to use. Molybdenum hexacarbonyl, dimolybdenum(II) tetraacetate, bis(cyclopentadienyl)-molybdenum(IV) dichloride, ferrocenium hexafluorophosphate, and NBu_4PF_6 were used as received from commercial sources. The ligands and complexes $^{mes}DAB^{H}$, $^{mes}DAB^{Me}$, $Mo(CO)_3(NCMe)_3$, $Mo(CO)_2(dppe)_2$, $Mo(O)_2(hoz)_2$, **4**, and **5** were prepared following literature procedures.[30−36]

NMR spectra were recorded on Bruker ARX 400 MHz spectrometers using solvent proton resonance peaks as references. IR spectra were recorded using a Thermo-Nicolet FTIR with attenuated total reflectance (ATR). UV/vis spectra were collected on a Shimazdu 2501 series spectrophotometer. Electron paramagnetic resonance (EPR) spectra were collected on a Bruker EMX spectrophotometer equipped with an Oxford Instruments liquid-helium continuous-flow cryostat. Spectra were obtained using 9.4 GHz frequency with 100 kHz field modulation.

X-ray Absorption Spectroscopy (XAS) Data Collection and Analysis. Mo K-edge (20.000 keV) XAS measurements were conducted on the insertion devise beamline of the Materials Research Collaborative Access Team (MRCAT, 10-ID) at the Advanced Photon Source (APS), Argonne National Laboratory. Ionization chambers were optimized for the maximum current with linear response (ca. 10^{10} photons detected per second) using 65% dinitrogen and 35% argon (10% absorption) in the incident X-ray detector and a mixture of argon (25% absorption) in the transmission X-ray detector. A third detector in the series simultaneously collected a Mo foil reference spectrum with each measurement for energy calibration. The X-ray beam was 0.8 × 0.8 mm, and data were collected in transmission geometry from 250 eV before the edge to 1000 eV beyond the edge in fast scan mode in about 5 min.

The energy of the preedge in the Mo K-edge XANES was used to determine the oxidation state of the samples and was calibrated from the position of standards. Because several of the samples were air-sensitive, all samples were prepared in a glovebox under air- and water-free conditions. The samples were diluted with dry SiO_2, ground to a uniform composition to about 5% Mo, and pressed into a self-supporting wafer. Six samples were gently pressed into a cylindrical sample holder consisting of six wells. The sample thickness was adjusted to give an absorbance (μx) of approximately 2 in the Mo edge region and an edge step ($\Delta\mu x$) of approximately 1. The sample holder with six samples was placed in a quartz tube (1 in. o.d. and 10 in. length) sealed with Kapton windows by two ultratorr fittings. A ball valve, welded to each ultratorr fitting, served to isolate the samples from air.

The energy of the preedge peak was determined from the maximum in the first derivative of the first peak in the leading edge of the XAS spectrum after calibration of the Mo foil for that spectrum. Standard procedures based on *WINXAS 3.1* software were used to normalize the XAS data using linear and cubic fits in the preedge and postedge regions of the spectra.

Electrochemistry. FTIR spectroelectrochemistry was conducted on a Bruker tensor-27 with a Remspec fiber-optic probe equipped with a low-temperature accessory. A platinum disk electrode was used as the working electrode, and a silver wire in CH_2Cl_2 was used as the reference electrode.[37]

A PARSTAT 2273 potentiostat−galvanostat was used in all of the voltammetric experiments in dichloromethane. A silver wire immersed in 0.010 M $AgNO_3$/0.10 M n-Bu_4NPF_6/acetonitrile and served as a reference electrode. The working electrode was glassy carbon with an area of 0.0706 cm^2. The potential of the silver working electrode was frequently measured with respect to the ferrocenium/ferrocene couple (Fc/Fc^+) in the solvent used, and all potentials are reported versus Fc^+. For scan rate studies, the specific scan rates that were chosen allowed for an approximately linear variation in $\log(\nu)$: ν = 0.1, 0.2, 0.3, 0.5, 1.0, and 2.0 V s^{-1} [$\log(\nu) = -1, -0.699, -0.523, -0.301, 0$, and 0.301].

Simulations were carried out using *DigiElch 4.M*, a software package for the *digi*tal simulation of common electrochemical experiments (http://www.elchsoft.com). When matching simulations with the experimental voltammograms, the objective was to find the single set of parameter values that provided the best average agreement between simulation and experiment for the entire range of scan rates that were employed. This means that a simulation at a given scan rate might be improved by some variation of one or more simulation parameter values, but this would lower the average goodness of fit for the entire set of voltammograms.

X-ray Crystallography. Detailed information concerning data collection and software used in analysis of the data can be found in the Supporting Information. Table 1 summarizes the crystallographic parameters for complexes **1** and **3**−**5**.

Synthesis of *cis*-$Mo(CO)_2(^{mes}DAB^{H})_2$ (1) and *cis*-$Mo(CO)_2(^{mes}DAB^{Me})_2$ (3). To a solution of *fac*,*fac*-$Mo(CO)_3(MeCN)_3$ was added 2 equiv of the corresponding DAB ligand, and the resulting solution was allowed to reflux for 6 h under a nitrogen blanket. The solvent was removed under vacuum, dissolved in a minimal volume of toluene, and recrystallized by the slow vapor diffusion of hexane.

1. Yield (0.1752 g): 75%. ^{1}H NMR (C_6D_6, 20 °C): δ 7.31 (s, 2H), 7.05 (s, 2H), 6.79 (s, 2H), 6.70 (s, 6H), 2.24 (s, 6H), 2.07 (s, 6H),

dx.doi.org/10.1021/ic400348j | Inorg. Chem. 2013, 52, 5457−5463

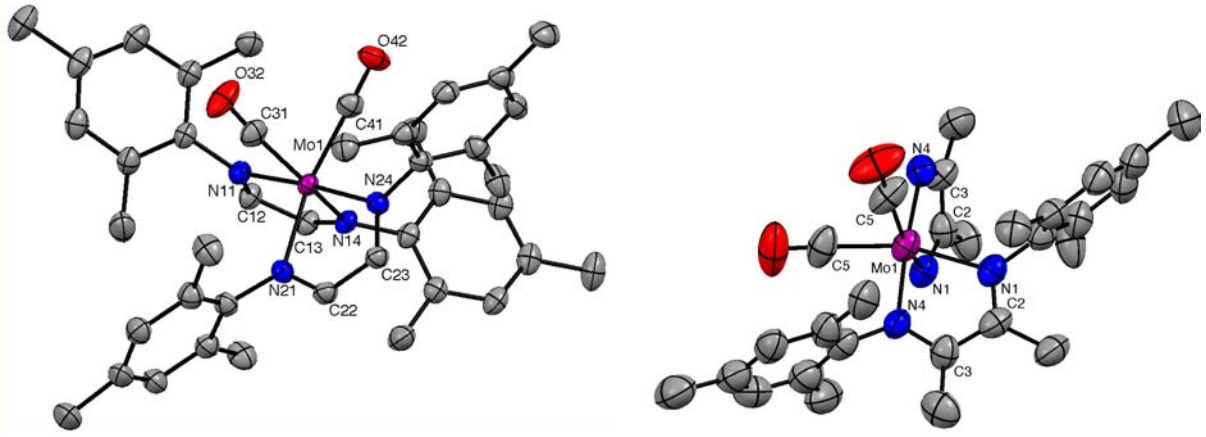

Figure 1. ORTEP-style X-ray molecular structures of **1** and **3** displayed at 50% probability. The molybdenum atom is purple and oxygen atoms are red, nitrogen atoms blue, and carbon atoms gray, with hydrogen atoms and two of the mesityl groups from **3** omitted for clarity. Crystallographically important bond distances (Å) [calculated by DFT]: (**1**) N11−C12 = 1.338(6) [1.352]; N14−C13 = 1.333(6) [1.347]; C12−C13 = 1.389(6) [1.408]; N21−C22 = 1.336(6) [1.347]; N24−C23 = 1.339(6) [1.354]; C23−C24 = 1.394(6) [1.407]; (**3**) N1−C2 = 1.307(6); N4−C3 = 1.343(6); C2−C3 = 1.377(7).

1.92 (s, 12H), 1.84 (s, 6H), 1.58(s, 6H). IR (solid ATR): ν(CO) 1928, 1853 cm^{-1}. ESI-MS: m/z 739. Anal. Calcd for $C_{42}H_{48}MoN_4O_2$: C, 68.46; H, 6.57; N, 7.60. Found C, 66.07; H, 5.86, N, 6.97.

3. Yield (0.2698 g): 85%. ^{1}H NMR ($CDCl_3$, 20 °C): δ 6.99 (s, 4H), 6.89 (s, 4H), 2.33 (s, 6H), 2.29 (6H), 2.15 (s, 12H), 2.07 (6H), 2.03 (6H), 2.00 (12H). IR (solid ATR): ν(CO) 1928, 1853 cm^{-1}. ESI-MS: m/z 794. Anal. Calcd for $C_{46}H_{56}MoN_4O_2$: C, 69.68; H, 7.12; N, 7.07. Found C, 72.24; H, 7.50; N, 7.03.

RESULTS AND DISCUSSION

Structural Characterization. Complex **1** crystallizes into space group $P\bar{1}$ and complex **3** into $P2/n$. Both complexes exhibit slightly distorted octahedral coordination environments. The interesting crystallographic features of the complexes lie within the DAB ligand C−N and C−C bonds. They exhibit elongated C−N bonds from the free ligand, with bond lengths averaging 1.33 Å and shortened C−C backbone bond lengths averaging 1.39 Å. For comparison, the same C−C and C−N bonds in complexes **4** and **5** average 1.47 and 1.3 Å in length, respectively. On the basis of the crystal structure alone, it would appear that each ligand would fit the partially reduced monoanionic motif, iminate π radical (1−). ^{1}H NMR spectra of **1** and **3** yield sharp, well-defined peaks in the diamagnetic region and integrate to the appropriate number of corresponding protons, indicating an S = 0 ground state. Furthermore, both complexes show no signal in the X-band EPR spectrum. Molecular structures of **1** and **3** along selected bond lengths are shown in Figure 1.

Mo K-Edge XAS. In order to assign an oxidation state to the title complexes, Mo K-edge energies were compared to a variety of molybdenum coordination complexes with varying oxidation states (Table 2). Plotting the formal oxidation states versus the edge energies gave a linear correlation. Having established the relationship between the oxidation state and edge energy for molybdenum complexes of unambiguous oxidation state, it was straightforward to make the assignment for the complexes *cis*-$Mo(CO)_2(DAB)_2$ reported herein. There is a consistent 5 eV per two oxidation states increase in the K-edge energy. With the K-edge energies for **1** and **3** being fairly close to the molybdenum(0) standards (Table 2), the oxidation state assignment for **1** and **3** is decisively molybdenum(0). The

Table 2. K-Edge Energies for Molybdenum Coordination Complexes

complex	Mo K-edge energy/keV	oxidation state
cis-$Mo(CO)_2(dppe)_2$	20.0001	0
$Mo_2(CH_3CO_2)_4$	20.0056	2+
$(Cp)_2MoCl_2$	20.0092	4+
$Mo(O)_2(hoz)_2$[a]	20.0140	6+
cis-$Mo(CO)_2(^{mes}DAB^{H})_2$ (**1**)	20.0007	0
cis-$Mo(CO)_2(^{mes}DAB^{Me})_2$ (**3**)	20.0002	0
$Mo(CO)_4(^{mes}DAB^{Me})$ (**4**)	20.0001	0
$Mo(CO)_3(CH_3CN)(^{mes}DAB^{H})$ (**5**)	20.0003	0

[a]Hoz = 2-(2′-hydroxyphenyl)oxazoline.

XANES spectra for **1** and **3** are displayed in Figure 2 alongside the standard $Mo(CO)_2(dppe)_2$.

Density Functional Theory (DFT) Calculations. In an attempt to better understand the observed changes in the DAB C−N and C−C bond lengths, a molecular orbital (MO) analysis was performed. Using the single-crystal X-ray structure for the starting geometry of complex **1**, geometry optimization was carried out employing unrestricted wave functions at the B3LYP/LanL2DZ[38,39] level of theory, utilizing the *Gaussian 09* suite of programs.[40] Calculated bond lengths are compared to experimental values from the X-ray structure in Figure 1, and they agree within experimental error. Analysis of the highest occupied molecular orbital (HOMO) and HOMO−1, which are nearly isoenergetic, demonstrates extensive delocalization of the four highest-energy electrons, as depicted in Figure 3. The orbitals comprising these span both DAB ligands and the metal center. The calculations predict that the most likely reasons for the observed changes in the DAB bond lengths are due to the C−C orbitals being π bonding in character and the N−C orbitals having antibonding character. The high covalent nature and delocalization of these frontier orbitals are responsible for the observed bond changes in the solid state rather than a formal oxidation at the molybdenum center and reduction of the DAB ligand.

Electronic Spectrum. Complexes **1** and **3** are intensely colored. The UV/vis spectrum of **1** is shown in Figure 4. The absorption in the visible at λ_{max} = 560 nm exhibits a large

dx.doi.org/10.1021/ic400348j | Inorg. Chem. 2013, 52, 5457−5463

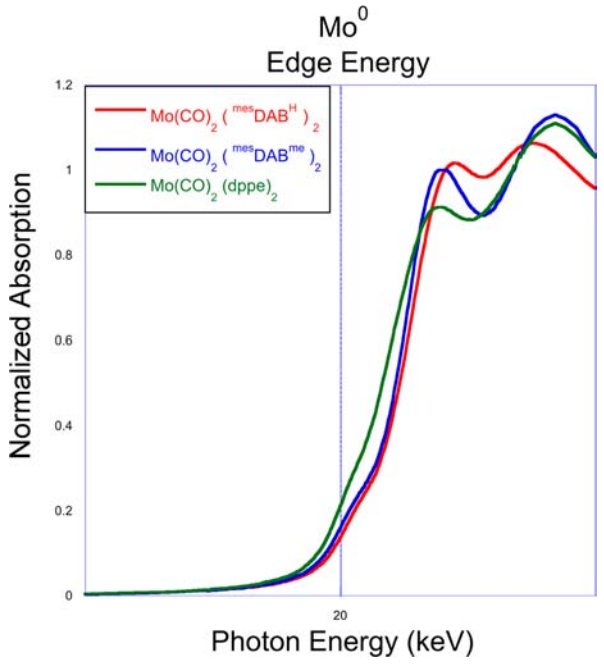

Figure 2. Molybdenum XANES spectra showing K-edge energies. Blue: $Mo(CO)_2(^{mes}DAB^H)_2$. Red: $Mo(CO)_2(^{mes}DAB^{me})_2$. Green: $Mo(CO)_2(dppe)_2$.

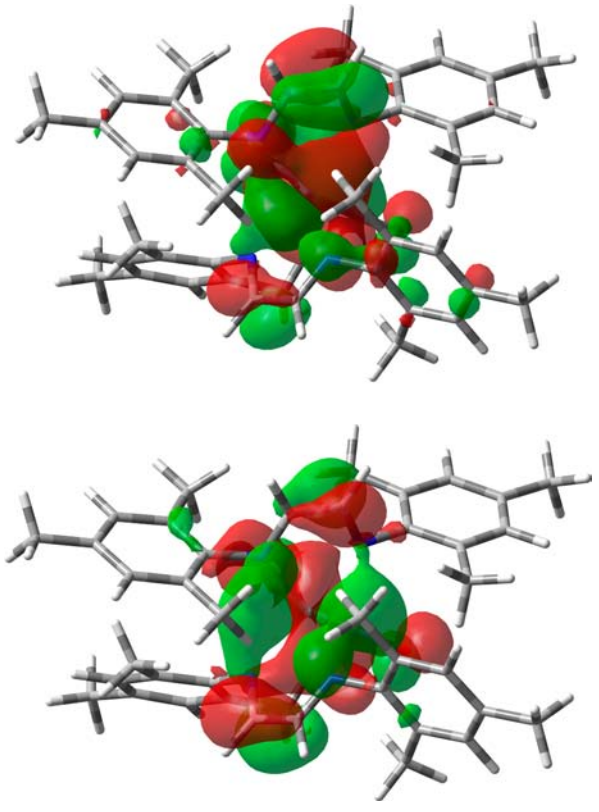

Figure 3. HOMO (top) and HOMO−1 (bottom) of complex **1** from DFT calculations. MO isovalue = 0.0200; density = 0.0040 for both cases.

extinction coefficient (ε = 18000 L mol^{-1} cm^{-1}), indicative of a charge-transfer (CT) transition. Time-dependent DFT (TD-DFT) revealed that transitions from the HOMO, HOMO−1, and HOMO−2 to the LUMO and LUMO+1 compose the CT

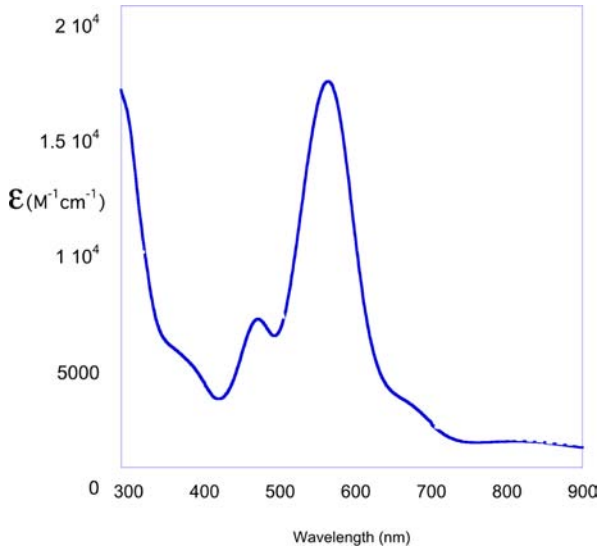

Figure 4. UV/vis spectrum of complex **1** in toluene.

band at 560 nm (Figure 5). The HOMO, HOMO−1, and HOMO−2 are significantly metal in character (approximately

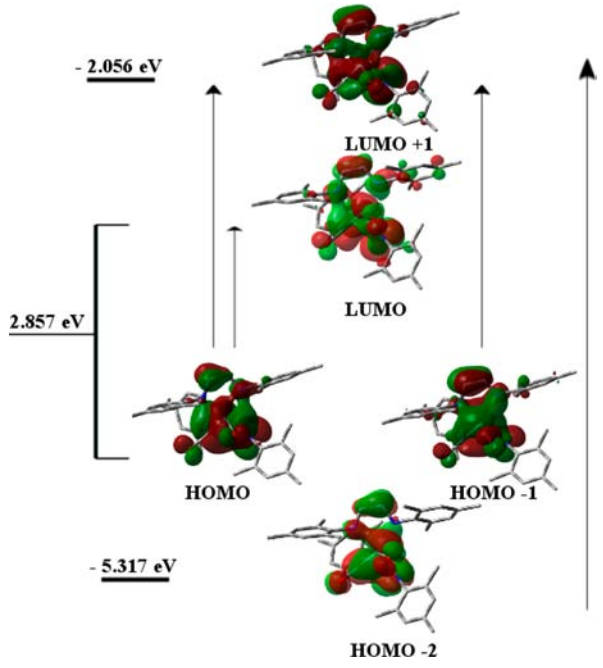

Figure 5. Relative energies of HOMO−2 through LUMO +1 and transitions comprising the MLCT band at 560 nm, as determined by TD-DFT. Orbital contributions: HOMO, Mo = 0.44, DAB = 0.42, COs = 0.14; HOMO−1, Mo = 0.46, DAB = 0.45, COs = 0.17; HOMO−2, Mo = 0.46, DAB = 0.37, COs = 0.17; LUMO, Mo = 0.16, DAB = 0.75, COs = 0.09; LUMO+1, Mo = 0.22, DAB = 0.61, COs = 0.17.

80%), and they have the same symmetry as the LUMO and LUMO+1, which are significantly $^{mes}DAB^H$ π^* in character. Therefore, the transition at 560 nm can be assigned to a metal-to-ligand charge transfer (MLCT).

Electrochemical Studies. Slow-scan cyclic voltammetry indicated an almost irreversible oxidation process with a peak potential of −0.084 V vs Fc/Fc^+ and an irreversible reduction process at −0.721 V vs Fc/Fc^+, which are directly related to

dx.doi.org/10.1021/ic400348j | Inorg. Chem. 2013, 52, 5457−5463

each other, as determined by varying scan rates. Figure 6 exemplifies a cyclic voltammogram at lower scan rates. At 0.1 V

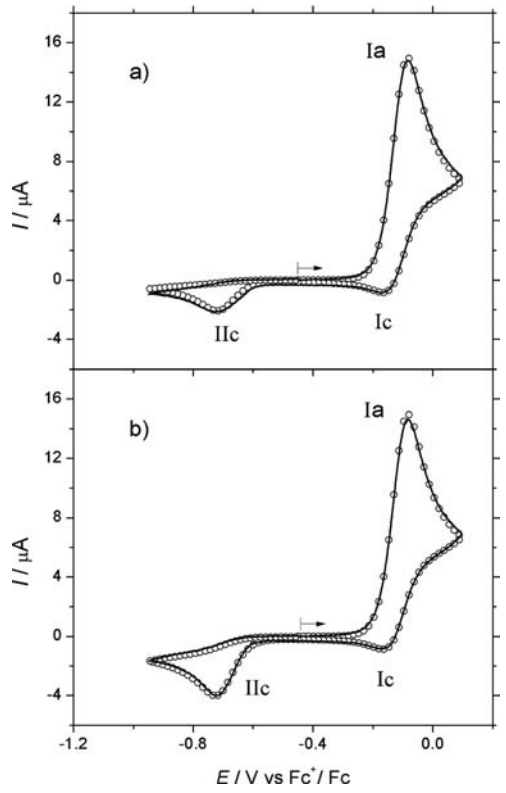

Figure 6. Background-corrected cyclic voltammograms of 1.0 mM complex **1** in dichloromethane with 0.30 M n-Bu_4NPF_6 (solid black line) at 0.1 V s^{-1} (resistance compensation = 150 Ω): (a) recorded without CO; (b) recorded in a CO saturated solution. Simulations (circles) are based on the reactions and parameters described in Table SI-1 in the Supporting Information. All of the voltammograms were recorded at 25 °C and 1 atm of pressure.

s^{-1}, peak Ia is almost irreversible but becomes fully reversible at scan rates greater than 3 V s^{-1}. The height of peak Ia corresponds to a one-electron oxidation. As the scan rate is increased, peak IIc disappears, suggesting that the species reacting at IIc is formed by some reaction of the cation formed at Ia. For peak Ia, the simulation showed good agreement with the experimental data considering a first-order coupled reaction of $\mathbf{1}^+$ in the forward direction, but it was not clear about the reaction order in the backward direction and perhaps the forward reaction involves the loss of carbon monoxide (CO). Figure 6b, conducted under a CO atmosphere, indicates no additional changes for peak Ia, but the reduction wave (IIc) has some dependence on CO, yielding more reduction current. This observation suggests that the oxidized species undergoes some CO loss and that this is suppressed when the solution is saturated with CO.

In differential FTIR spectroelectrochemistry experiments, two new species were observed. Figure 7 (solid line, a) indicates the disappearance of the two peaks at 1928 and 1853 cm^{-1} due to **1** when the spectrum was recorded with the potential held at peak Ia (Figure 6). The product that is formed, $\mathbf{2}^+$, gives a single peak at 1900 cm^{-1}, which indicates the formation of a *trans*-dicarbonyl species. To rule out dissociation of CO, the reduction of $\mathbf{2}^+$ was followed by difference IR. Figure 7 (dashed line, b) demonstrates the

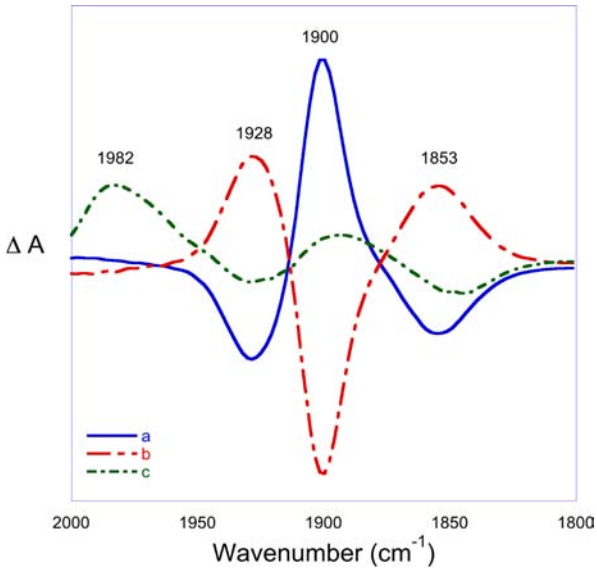

Figure 7. Difference FTIR spectroelectrochemistry of complex **1**: (solid line, a) background taken with no applied potential and the electrode potential held at peak Ia during spectral scans; (dashed line, b) electrode potential held at peak Ia during background scans and at peak IIc during spectral scans; (dotted line, c) background taken with no applied potential and the electrode potential held at peak Ia during spectral scans at −78 °C. Negative peaks indicate the starting material; positive peaks indicate the products. The electrode potential at peak Ia was 0.40 V and that at peak IIc −0.40 V vs Ag/AgCl. Data obtained in CH_2Cl_2 containing 1.3 mM **1** and 0.17 M n-Bu_4NPF_6 and purged with argon.

change that occurs upon the reduction of $\mathbf{2}^+$, the disappearance of the single peak at 1900 cm^{-1}, and the reappearance of the two peaks of **1** at 1928 and 1853 cm^{-1}. Without added CO, the diffusion of free CO from the electrode surface to the bulk solution would be fast enough to prevent re-formation of the *cis*-dicarbonyl complex **1**. Thus, the absence of any new peaks demonstrates that isomerization is the dominant process, and it is indeed reversible. It is apparent that, upon oxidation, $\mathbf{1}^+$ forms the *trans*-dicarbonyl isomer $\mathbf{2}^+$. The latter exhibits only one stretching frequency in the IR region, as would be expected for an octahedral *trans*-dicarbonyl species. The X-band EPR spectrum of the oxidation product of **1** (Figure 8) is consistent with a metal-centered oxidation, with the oxidation state being the molybdenum(I), $S = {}^1/_2$, complex.[14,41−44] The spectrum is in agreement with the notion that the observed oxidation occurs at the metal center.

In an attempt to capture $\mathbf{1}^+$ (oxidized molybdenum with *cis*-dicarbonyl), we conducted the spectroelectrochemistry experiment at low temperature in a dry ice/acetone bath (−78 °C). Figure 7 (dotted line, c) shows the IR spectrum of [*cis*-$Mo(^{mes}DAB^H)_2(CO)_2]^+$ ($\mathbf{1}^+$). At −78 °C, isomerization to the *trans*-dicarbonyl $\mathbf{2}^+$ isomer is slow enough to allow observation of $\mathbf{1}^+$. The carbonyl stretching frequencies in $\mathbf{1}^+$ shift to higher frequencies by ca. 50 cm^{-1} compared to **1**. This shift in the stretching frequency along with isomerization, which has been rationalized theoretically for other molybdenum dicarbonyl complexes, is consistent with a metal-centered oxidation.[45]

All of the data in hand was used to construct a square scheme for the observed reactivity (Scheme 2). Complex **1** undergoes a reversible oxidation at E°_1 of −0.112 V vs Fc/Fc^+ to form $\mathbf{1}^+$, [*cis*-$Mo(CO)_2(^{mes}DAB^H)_2]^+$. The rate at which $\mathbf{1}^+$ undergoes cis-to-trans isomerization to give $\mathbf{2}^+$ has been determined by

dx.doi.org/10.1021/ic400348j | Inorg. Chem. 2013, 52, 5457−5463

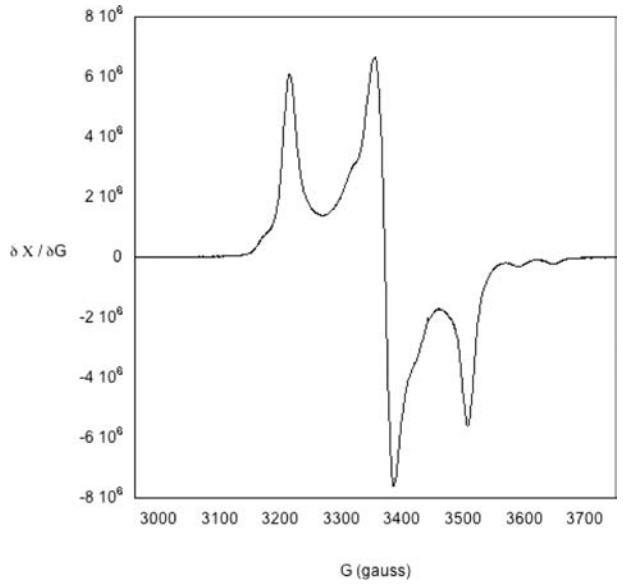

Figure 8. X-band EPR spectrum of the oxidation product of **1** ($\mathbf{2}^+$) recorded at 125 K as CH_2Cl_2 glass. g_{avg} = 2.0027, g_x = 2.0945, g_y = 1.9965, g_z = 1.9199. $A(^{95}\text{Mo}/^{97}\text{Mo})$ = 28 G.

Scheme 2. Square Scheme Used To Fit the Cyclic Voltammetry Data for Complex 1[a]

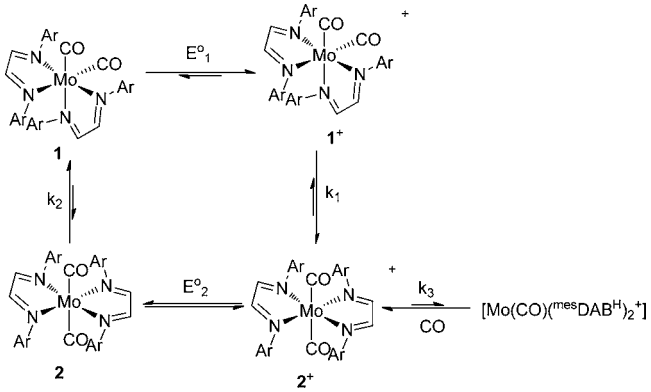

[a] E°_1 = −0.112 V vs Fc/Fc^+; E°_2 = −0.683 V vs Fc/Fc^+; k_1 = 1.2 s^{-1}; k_2 ≥ 10 s^{-1}; k_3 = 0.12 s^{-1}. See the Supporting Information for more details regarding the simulation parameters.

simulations, k_1 = 1.2 s^{-1} at 25 °C. Complex $\mathbf{2}^+$ can be reversibly reduced to form the trans neutral complex **2** at E°_2 of −0.683 V versus Fc/Fc^+. Isomerization of **2** back to **1** occurs rapidly with k_2 > 10 s^{-1}. The rate constant of carbonyl dissociation from $\mathbf{2}^+$ has been determined to be k_3 = 0.12 s^{-1}. In addition, the cyclic voltammetry experiments also revealed the presence of two consecutive oxidation peaks at higher anodic potentials, IIIa (a reversible peak) and IVa (an irreversible peak) in Figure SI-9 in the Supporting Information. Peak IIIa is prevalent at low scan rates, but its height, relative to peak IVa, decreases as the scan rate increases. This observation suggests that peak IIIa is due to oxidation of the ultimate product at peak Ia, $\mathbf{2}^+$. Peak IVa (peak potential 0.914 V vs Fc/Fc^+ at 2.0 V s^{-1}), which is prevalent at rapid scan rates, is assumed to be due to oxidation of the initial product formed at peak Ia, $\mathbf{1}^+$. The fact that peak IVa is chemically irreversible at all scan rates is consistent with a rapid decomposition of the reputed $\mathbf{1}^{2+}$.

CONCLUSION

In summary, new molybdenum complexes with two coordinated DAB ligands have been synthesized and fully characterized. Cyclic voltammetry studies show oxidation followed by a chemical change, affording a new species that reverts to the starting complex upon reduction. FTIR spectroelectrochemistry has identified a reversible cis-to-trans isomerization of the oxidized complex $[Mo(CO)_2(^{mes}DAB^{H/Me})]^+$ as the chemical process. An excellent fit of the cyclic voltammetry data was obtained based on the square scheme shown in Scheme 2, allowing determination of the corresponding potentials and rate constants. Mo K-edge XAS data established the oxidation state of the metal center as molybdenum(0). While there are many examples of DAB complexes where the bond lengths can be useful in oxidation state assignment, the title complexes do not follow that particular trend. Serendipitously, the bond lengths as established by X-ray crystallography coincide exactly with the established π-radical ligand.

ASSOCIATED CONTENT

Supporting Information

X-ray crystallographic data in CIF format, experimental prodcedures, ORTEP diagrams, bond lengths and angles, additional spectra, cyclic voltammograms, electrochemical simulation parameters, calculated HOMO and LUMO, supporting references, and XYZ coordinates. This material is available free of charge via the Internet at http://pubs.acs.org.

AUTHOR INFORMATION

Corresponding Author

*E-mail: mabuomar@purdue.edu (M.M.A.-O.), evansd@purdue.edu (D.H.E.).

Present Address

‡Department of Chemistry, Temple University, Philadelphia, PA 19122.

Notes

The authors declare no competing financial interest.

ACKNOWLEDGMENTS

Funding for this research was provided by U.S. Department of Energy, Office of Basic Energy Sciences (DOE-BES; Grant DE-FG-02-06ER15794 to M.M.A.-O.), and the NSF (Grant CHE-0715375 to D.H.E.). Use of the APS was supported by the DOE-BES under Contract DE-AC02-06CH11357. MRCAT operations are supported by the Department of Energy and the MRCAT member institutions. Partial funding for J.T.M. was provided by the Chemical Sciences, Geosciences and Biosciences Division, U.S. Department of Energy, under Contract DE-AC0-06CH11357.

REFERENCES

(1) Bart, S. C.; Chłopek, K.; Bill, E.; Bouwkamp, M. W.; Lobkovsky, E.; Neese, F.; Wieghardt, K.; Chirik, P. J. *J. Am. Chem. Soc.* **2006**, *128*, 13901.

(2) Bart, S. C.; Lobkovsky, E.; Bill, E.; Wieghardt, K.; Chirik, P. J. *Inorg. Chem.* **2007**, *46*, 7055.

(3) Kaim, W.; Schwederski, B. *Coord. Chem. Rev.* **2010**, *254*, 1580.

(4) Ray, K.; Petrenko, T.; Wieghardt, K.; Neese, F. *Dalton Trans.* **2007**, 1552.

(5) Blackmore, K. J.; Lal, N.; Ziller, J. W.; Heyduk, A. F. *Eur. J. Inorg. Chem.* **2009**, *2009*, 735.

(6) Lionetti, D.; Medvecz, A. J.; Ugrinova, V.; Quiroz-Guzman, M.; Noll, B. C.; Brown, S. N. *Inorg. Chem.* **2010**, *49*, 4687.
(7) Lippert, C. A.; Soper, J. D. *Inorg. Chem.* **2010**, *49*, 3682.
(8) Smith, A. L.; Clapp, L. A.; Hardcastle, K. I.; Soper, J. D. *Polyhedron* **2010**, *29*, 164.
(9) Haneline, M. R.; Heyduk, A. F. *J. Am. Chem. Soc.* **2006**, *128*, 8410.
(10) Stanciu, C.; Jones, M. E.; Fanwick, P. E.; Abu-Omar, M. M. *J. Am. Chem. Soc.* **2007**, *129*, 12400.
(11) Tsurugi, H.; Saito, T.; Tanahashi, H.; Arnold, J.; Mashima, K. *J. Am. Chem. Soc.* **2011**, *133*, 18673.
(12) Guan, Z.; Popeney, C. S. *Top. Organomet. Chem.* **2009**, *26*, 179.
(13) Kaneko, H.; Nagae, H.; Tsurugi, H.; Mashima, K. *J. Am. Chem. Soc.* **2011**, *133*, 19626.
(14) Stoffelbach, F.; Poli, R.; Maria, S.; Richard, P. *J. Organomet. Chem.* **2007**, *692*, 3133.
(15) Gibson, V. C.; O'Reilly, R. K.; Reed, W.; Wass, D. F.; White, A. J. P.; Williams, D. J. *Chem. Commun.* **2002**, 1850.
(16) Gibson, V. C.; O'Reilly, R. K.; Wass, D. F.; White, A. J. P.; Williams, D. J. *Macromolecules* **2003**, *36*, 2591.
(17) Le Grognec, E.; Claverie, J.; Poli, R. *J. Am. Chem. Soc.* **2001**, *123*, 9513.
(18) Arnaíz, F. J.; Bartolomé, C. S.; García, G.; Pérez, M. *Inorg. Chim. Acta* **1988**, *141*, 57.
(19) Finger, K.; Daniel, C. *J. Chem. Soc., Chem. Commun.* **1995**, 1427.
(20) Koten, G. V.; Vrieze, K. In *Advances in Organometallic Chemistry*; Stone, F. G. A., Robert, W., Eds.; Academic Press: New York, 1982; Vol. *21*, p 151.
(21) Muresan, N.; Lu, C. C.; Ghosh, M.; Peters, J. C.; Abe, M.; Henling, L. M.; Weyhermüller, T.; Bill, E.; Wieghardt, K. *Inorg. Chem.* **2008**, *47*, 4579.
(22) Ghosh, M.; Sproules, S.; Weyhermüller, T.; Wieghardt, K. *Inorg. Chem.* **2008**, *47*, 5963.
(23) Ghosh, M.; Weyhermüller, T.; Wieghardt, K. *Dalton Trans.* **2008**, 5149.
(24) Ghosh, P.; Bill, E.; Weyhermüller, T.; Neese, F.; Wieghardt, K. *J. Am. Chem. Soc.* **2003**, *125*, 1293.
(25) Kreisel, K. A.; Yap, G. P. A.; Theopold, K. H. *Inorg. Chem.* **2008**, *47*, 5293.
(26) Khusniyarov, M. M.; Weyhermüller, T.; Bill, E.; Wieghardt, K. *J. Am. Chem. Soc.* **2008**, *131*, 1208.
(27) Stoffelbach, F.; Rebière, B.; Poli, R. *Eur. J. Inorg. Chem.* **2004**, *2004*, 726.
(28) Oelkers, B.; Venker, A.; Sundermeyer, J. R. *Inorg. Chem.* **2012**, *51*, 4636.
(29) Han, Y. J.; Lees, A. J. *Inorg. Chim. Acta* **1988**, *147*, 45.
(30) Arduengo, A. J., III; Krafczyk, R.; Schmutzler, R.; Craig, H. A.; Goerlich, J. R.; Marshall, W. J.; Unverzagt, M. *Tetrahedron* **1999**, *55*, 14523.
(31) Johnson, R.; Madhani, H.; Bullock, J. P. *Inorg. Chim. Acta* **2007**, *360*, 3414.
(32) Tate, D. P.; Knipple, W. R.; Augl, J. M. *Inorg. Chem.* **1962**, *1*, 433.
(33) tom Dieck, H. K. E. *Z. Naturforsch., B: J. Chem. Sci.* **1982**, *37*, 324.
(34) Ardon, M.; Hogarth, G.; Oscroft, D. T. W. *J. Organomet. Chem.* **2004**, *689*, 2429.
(35) Bagherzadeh, M. T. L.; Latifi, R.; Ellern, A.; Woo, K. L. *Inorg. Chim. Acta* **2008**, *361*, 2019.
(36) Vlček, A., Jr. *Coord. Chem. Rev.* **2002**, *230*, 225.
(37) Shaw, M. J.; Henson, R. L.; Houk, S. E.; Westhoff, J. W.; Jones, M. W.; Richter-Addo, G. B. *J. Electroanal. Chem.* **2002**, *534*, 47.
(38) Becke, A. D. *Phys. Rev. A* **1988**, *38*, 3098.
(39) Li, J.; Shiota, Y.; Yoshizawa, K. *J. Am. Chem. Soc.* **2009**, *131*, 13584.
(40) Frisch, M. J.; Trucks, G. W.; Schlegel, H. B.; Scuseria, G. E.; Robb, M. A.; Cheeseman, J. R.; Scalmani, G.; Barone, V.; Mennucci, B.; Petersson, G. A.; Nakatsuji, H.; Caricato, M.; Li, X.; Hratchian, H. P.; Izmaylov, A. F.; Bloino, J.; Zheng, G.; Sonnenberg, J. L.; Hada, M.; Ehara, M.; Toyota, K.; Fukuda, R.; Hasegawa, J.; Ishida, M.; Nakajima, T.; Honda, Y.; Kitao, O.; Nakai, H.; Vreven, T.; Montgomery, J. A., Jr.; Peralta, J. E.; Ogliaro, F.; Bearpark, M.; Heyd, J. J.; Brothers, E.; Kudin, K. N.; Staroverov, V. N.; Kobayashi, R.; Normand, J.; Raghavachari, K.; Rendell, A.; Burant, J. C.; Iyengar, S. S.; Tomasi, J.; Cossi, M.; Rega, N.; Millam, J. M.; Klene, M.; Knox, J. E.; Cross, J. B.; Bakken, V.; Adamo, C.; Jaramillo, J.; Gomperts, R.; Stratmann, R. E.; Yazyev, O.; Austin, A. J.; Cammi, R.; Pomelli, C.; Ochterski, J. W.; Martin, R. L.; Morokuma, K.; Zakrzewski, V. G.; Voth, G. A.; Salvador, P.; Dannenberg, J. J.; Dapprich, S.; Daniels, A. D.; Farkas, Ö.; Foresman, J. B.; Ortiz, J. V.; Cioslowski, J.; Fox, D. J. *Gaussian 09*, revision B.01; Gaussian, Inc.: Wallingford, CT, 2010.
(41) Johnson, A. R.; Davis, W. M.; Cummins, C. C.; Serron, S.; Nolan, S. P.; Musaev, D. G.; Morokuma, K. *J. Am. Chem. Soc.* **1998**, *120*, 2071.
(42) Stoll, M. E.; Belanzoni, P.; Calhorda, M. J.; Drew, M. G. B.; Félix, V.; Geiger, W. E.; Gamelas, C. A.; Gonçalves, I. S.; Romão, C. C.; Veiros, L. F. *J. Am. Chem. Soc.* **2001**, *123*, 10595.
(43) McQuillan, F. S.; Green, T. L.; Hamor, T. A.; Jones, C. J.; Maher, J. P.; McCleverty, J. A. *J. Chem. Soc., Dalton Trans.* **1995**, 3243.
(44) Jose, D. A.; Shukla, A. D.; Ramakrishna, G.; Palit, D. K.; Ghosh, H. N.; Das, A. *J. Phys. Chem. B* **2007**, *111*, 9078.
(45) Mingos, M. P. *J. Organomet. Chem.* **1979**, *179*, C29.